Batteries & Supercaps

Research Article
doi.org/10.1002/batt.202400203

Chemistry Europe
European Chemical Societies Publishing

www.batteries-supercaps.org

Scalable Fabrication of Flexible Supercapacitor Electrodes Using Sustainable Water-Based Onion-Like Carbon Inks

Christian Bauer[+],[a] Tobias Neff[+],[a, b] Adam Day,[a, b] and Anke Krueger*[a, b]

The increasing usage of electrical energy storage solutions demands for cost effective, scalable and sustainable manufacturing technologies. Deposition of functional inks, carrying electrochemically active materials is a suitable technique as it delivers material with selected properties only to required locations. However, the production of stable dispersions featuring high concentrations of active material - necessary for effective deposition - is challenging. Here we present an approach to print supercapacitor electrodes with onion-like carbon as active material, using a simple, cost-effective process as well as a water-based ink. The ink is highly stable and can be deposited by spray and inkjet techniques. The fabricated electrodes offer a capacitance of up to 14 mF cm^{-2} (27 F g^{-1}) and retained 97% of their initial capacitance after 5000 cycles, demonstrating excellent performance and stability of the coating.

Introduction

The digital transformation with its accelerating number of decentralized electronic devices is powered by individual energy storage solutions.[1–2] The different sizes and geometries of such devices create an imminent need of individually adjustable power sources. Printing of those key parts is a promising and more flexible alternative to established slurry-based electrode manufacturing techniques. Furthermore, printing enables customized design and can be effectively integrated into the overall manufacturing processes.[3–7] Recently, functional inks were used to manufacture various devices like photodetectors,[8–9] gas and humidity sensors,[10–12] solar cells,[13–14] field effect transistors[15–16] as well as supercapacitors.[17–21] These are important components of decentral energy storage solutions. Energy is stored in them in an electric double layer formed between the electrolyte and an active material. This active material has to be electrochemically stable and needs to offer a high specific surface in combination with an open porosity to grant accessibility for the electrolyte.[22] Materials based on sp^2-hybridized carbon fulfill these requirements while maintaining a high degree of electric conductivity, necessary to deliver charge to the electrode surface, where the energy is stored in an electric field between the charged electrode and a layer of solvated ions.[23–24]

In this work, onion-like carbon (OLC) was chosen as active material due to its conductivity and open mesoporous structure,[25] which enables accessibility for the electrolyte even at elevated charging rates.[26] OLC can be produced from detonation nanodiamond[27] and other sources at large scale[28] and is considered environmentally benign and biocompatible.[29] Recently, OLC have also been used in supercapacitor and battery applications.[30–32]

However, to print electrodes, carbon materials need to be dispersed in the form of an ink, resulting in a colloidal suspension in which the solid particles are evenly distributed in the liquid phase. Dispersing carbon particles like OLC using common solvents is a challenge, because of interparticle interactions which promote agglomeration.[33] Additionally, the absence of functional groups that could interact with solvents or repulse other particles hinders suspension or solvation of OLC.[34–35] Inkjet printing has been used for the fabrication of supercapacitors e.g. using graphene-based inks.[21] However, OLC could not be used in printed devices so far. Different coating techniques such as electrophoretic deposition have been used instead.[20] A more detailed comparison of different carbon-based inks used with different coating techniques and the resulting performance parameters of the resulting supercapacitors is shown in the SI (Table S1).

Here we report on the production of a stable, environmentally friendly, water-based functional ink to produce supercapacitor electrodes using OLC as active material. The ink dispersion is designed to be stable for years and was studied by high-resolution transmission electron microscopy, dynamic light scattering and Raman microscopy. With inkjet printing and spray deposition, we report two different printing techniques to obtain thin film supercapacitor electrodes. The electrochemical performance and stability of the electrodes was demonstrated by cyclic voltammetry in a wide potential window and over 5000 cycles.

[a] C. Bauer,[+] T. Neff,[+] A. Day, A. Krueger
Institute for Organic Chemistry, Julius-Maximilian University Würzburg, Am Hubland, 97074 Würzburg, Germany

[b] T. Neff,[+] A. Day, A. Krueger
Institute of Organic Chemistry, University of Stuttgart, Pfaffenwaldring 55, 70569 Stuttgart, Germany
E-mail: anke.krueger@oc.uni-stuttgart.de

[+] These authors contributed equally.

Supporting information for this article is available on the WWW under https://doi.org/10.1002/batt.202400203

Experimental

Active Material Production and Milling

The active material OLC was obtained after thermal annealing of detonation nanodiamond (Gansu Lingyun Corp., China) and a heating rate of 5 K min^{-1} in vacuum (~1 mbar). The temperature was for kept two hours at 1500 °C in a tube furnace (STF 16/450, Carbolite Gero GmbH, Germany) and subsequently cooled down to room temperature with a rate of 5 K min^{-1}.[30] The temperature was controlled using a built-in digital temperature controller (3216 P1, Eurotherm, Germany). Prior to milling, OLC (3.0 g) and 1.8 g sodium dodecyl sulfate (SDS Sigma Aldrich, USA) were dispersed in deionized water (130.0 g) using an ultrasonic bath for 30 minutes. Milling of the dispersion was conducted for two hours under ambient conditions with an attrition mill (minicer, Netzsch, Germany) with a circumferential velocity of 10 m s^{-1} using zirconia milling beads (30–50 μm, Tosoh Corp., Japan), yielding a black dispersion with an amount of solid components of 3 wt%.[36]

Ink Preparation

For the spray printing, the OLC dispersion (2.0 g) and deionized water (4.0 g) were mixed in a ration 1 : 2 to obtain a mass continent of 1 wt%. For electrode production, the ink was sprayed using a small piezoceramic atomizer with a mesh size of 10 μm operated at 110 KHz using a small driver board (300 mA and 5 V). Carbon coated aluminum foil (Zflo 2653, Transcontinental Advanced Coatings, USA) was used as the substrate, which was kept at 100 °C.

To obtain the dispersion for inkjet printing, the OLC deionized water (4.0 g), dispersion (2.0 g) and DMSO (0.2 g) were mixed in a ratio 20 : 10 : 1. The ink was printed onto carbon coated aluminum foil (Zflo 2653, Transcontinental Advanced Coatings, USA), which was attached to a DIN A4 paper using a conventional ink jet printer (MFC 290 C, Brother, Japan) with a nozzle diameter of 30 μm. The deposition pattern was controlled by a computer. To calculate the Ohnesorge number (see SI), the dynamic viscosity of both inks was determined with a rolling-ball viscosimeter (Lovis 2000 ME, Anton Paar, Germany).

Substrates coated by both techniques were die cut with a punching iron and pressed with a hydraulic press (ca. 0.2 GPa) yielding round electrodes (16 mm diameter) with a mass loading of 0.5 mg cm^{-2} achieved by repeated printing cycles if needed.

Materials Characterization

Particle size in the dispersions was determined by dynamic light scattering (Zetasizer Nano ZS, Malvern, USA) using the Marquardt method. Data are presented as intensity and volume distribution (see SI). Zetapotential was measured in deionized water at the intrinsic pH value of the dispersion.

Specific surface areas were determined using BET isotherms using a Micro200C-01 volumetric analyzer (3P instruments, Germany). For sample preparation, the dispersion was freeze-dried using a lyophylizator, to prevent irreversible clogging of pores. Prior to measurement, the sample was degassed at 150 °C under high vacuum for 24 h. The measurements were conducted at 77 K using nitrogen as adsorbent. For further calculations, a model for slit shaped micropores was used.

For high-resolution electron transmission microscopy (HRTEM), the ink was drop casted onto a copper grid coated with a lacey carbon film (Plano GmbH). The measurement was conducted using a FEI Titan 80–300 (Thermo Fischer Scientific Inc., USA) with an operating voltage of 300 kV. Scanning electron microscopy (SEM) images were recorded at an operating voltage of 5 kV using a Gemini Fe-SEM Ultra-plus Zeiss field emission scanning electron microscope (Carl Zeiss, Germany). The electrodes were attached by conductive carbon tapes without further preparation. Raman spectra were measured with a DXR Raman microscope (Thermo Fisher Scientific Inc., USA), using a laser power of 0.02 mW and an excitation wavelength of 532 nm.

Electrochemical Characterization

All electrodes were transferred into a drying furnace (130 °C). For electrochemical measurements, symmetrical supercapacitors were built using a stainless-steel test cell (ECC-Ref, El-Cell, Germany) separated by a polymer membrane (Cellgard 2325, El-Cell, Germany). For the electrolyte, a 1 M solution of tetraethyl ammonium tetra-fluoroborate ($TEABF_4$; TCI, Germany) in acetonitrile (CH_3CN, Sigma Aldrich, USA) was used. For each deposition technique, three test cells were assembled in the absence of humidity (< 1 ppm) and oxygen (< 1 ppm) using a glovebox (N_2, Labmaster 130, M. Braun Inertgas-Systeme, Germany). Potentiostatic techniques including cyclic voltammetry (CV) and electrochemical impedance spectroscopy (EIS) were performed using a potentio-/galvanostat VMP300 (Bio-Logic Instruments, France). CV measurements were carried out over the voltage range of ±2.5 V at different scan rates ranging from 0.02 V s^{-1} to 50 V s^{-1}. For long-term stability tests, 5000 charge/discharge cycles were performed at a scan rate of 2.5 V s^{-1}. All electrochemical measurements have been carried out in triplicates and were highly reproducible.

For each applied scan rate the arithmetic average of ten consecutive cycles was used to calculate the total capacitance of the device C_{CV} (Eq. 1) as well as the specific capacitance for one electrode C_E (Eq. 2), where a is the area of one electrode, I the current, v the scan rate and V_0 the potential window:

$$C_{CV} = \frac{\int_0^{V_0} I(t)^* dV}{2^* V_0^* v} \quad (1)$$

$$C_E = \frac{2^* C_{CV}}{a} \quad (2)$$

Results and Discussion

The successful deposition of ink strongly relies on the preparation of a homogeneous and stable dispersion, wherein the ink components are uniformly distributed. Pristine OLC dispersions without treatment or additives form aggregates and precipitate completely from the dispersion within minutes. To increase the stability of the dispersion and to reduce the particle size in order to avoid clogging of the nozzle during deposition, it was necessary to disperse the OLC aggregates. As reported in literature, the attracting forces between primary particles are not only explained by π–π stacking between single OLC but also by covalent bonds that are connecting the particles. These bonds between OLC form during the high temperature fabrication resulting in interconnecting necks between spherical OLC.[25,35] To break these interparticle connections, the energy input provided by an attrition mill is required, as already shown for a dispersion of detonation nanodiamonds[37] To prevent reagglomeration of the OLC, additional measures are necessary to stabilize the dispersion.

Research Article
doi.org/10.1002/batt.202400203
Chemistry Europe
European Chemical Societies Publishing

This can be achieved by surface functionalization by oxidation or fluorination.[38] Another strategy to increase the dispersibility of OLC is to introduce stabilizing additives like polyacrylic acid.[34] To maintain electrochemical stability of the resulting electrodes while achieving a suitable concentration of active material for printing, sodium dodecyl sulfate (SDS) was employed as surfactant, for other carbon materials.[39–40] Here, we use 0.6 wt% of SDS in water in combination with the milling process to stabilize 1 wt% of OLC (Figure 1A) to form a stable and sustainable OLC ink.

Milling of OLC in water in the presence of SDS resulted in a stable black dispersion. Freshly generated deagglomerated OLC particles are stabilized in situ by the surfactant molecules.[41] The obtained dispersion featuring milled OLC with a particle mean size of 76.1 nm in a range between 30 and 300 nm (Figure 1B left) and a ζ-potential of −30,3 mV (pH 8.3). The dispersion remains stable for over two years, showing a remarkable stability, with only a slight increase of the mean particle size (Fig S3). When considering a agglomerate size between 400 and 1000 nm of pristine OLC,[33] the milling process significantly reduces the size of OLC agglomerates. This reduction in size of OLC and the stability of the ink are crucial for ensuring its printability. The use of a surfactant such as SDS, is essential because milled OLC without SDS does not yield a stable dispersion, leading to particle reagglomeration (Figure 1B left).

The specific surface, determined using the Brunauer-Emmett-Teller method (BET), changed from around 389 $m^2\ g^{-1}$ for pristine OLC to 220 $m^2 g^{-1}$ for the milled dispersion (Figure S5). The decrease of specific surface after milling of OLC is due to the partial clogging of pores by milling induced debris,[42] and is further promoted by a significant amount of SDS remaining after removal of the liquid by freeze drying. Freeze-drying of the dispersion prevents the irreversible agglomeration of secondary particles and possible clogging of pores that would occur during a thermal drying process. A

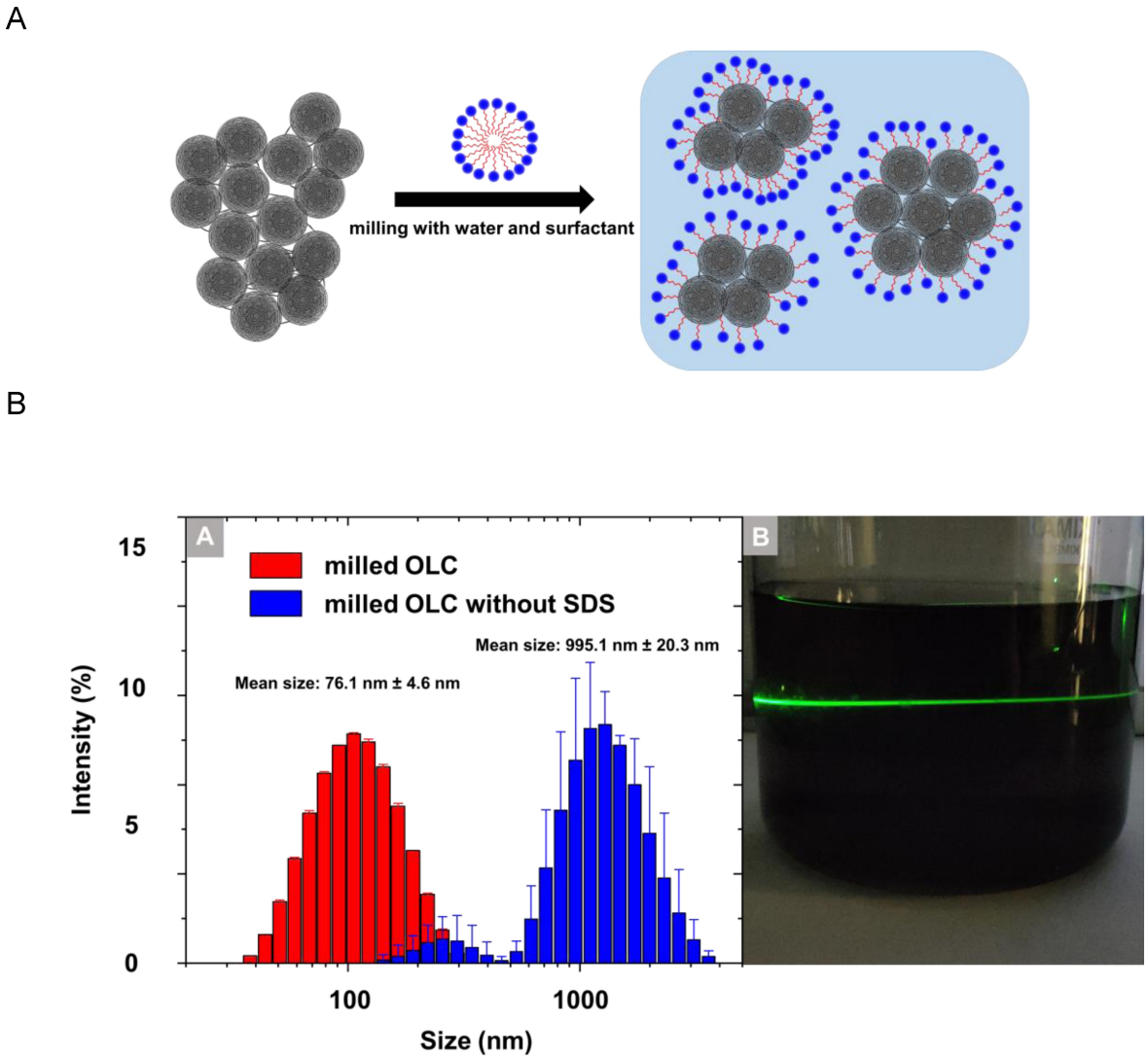

Figure 1. A) Deagglomeration of onion-like carbon by attrition milling and simultaneous stabilization of the aqueous dispersion by sodium dodecyl sulfate forming a mediating layer at the solid to liquid interface; B) Particles size distribution measured by dynamic light scattering of the milled dispersion with and without SDS (left) and colloidal dispersion demonstrated by the Tyndall effect (right).

Research Article
doi.org/10.1002/batt.202400203
Chemistry Europe
European Chemical Societies Publishing

redispersion of a freeze-dried dispersion, offering possibilities for process engineering was tested, but did yield a dispersion with two different particle size fractions (Figure S1). Milling of OLC was also performed without surfactant but led to an unsatisfying dispersion, where the active material OLC precipitated within minutes (Figure 1B left). Eventually, a concentration of surfactant of at least 0.6 wt% was necessary to maintain a sufficient weight fraction (1 wt%) of OLC in dispersion. Milling of OLC with SDS provided excellent colloidal stability (Figure 1B right).

Milling of particles not only reduces the specific surface and size of the agglomerates but can also damage of the particle structure potentially deteriorating the properties of the electrode which has been reported for carbon nanotubes.[43] Especially surfactants can promote the exfoliation of carbon layers and further degradation of the particle structure during milling.[44]

To investigate the structural influence of milling, OLC were examined before and after mechanochemical deagglomeration in the presence of SDS by Raman spectroscopy as well as HRTEM measurements (Figure 2).

In the Raman spectra, the intensity ratio of the D and G band for pristine OLC of 1.06 (1/0.94) increases to 1.16 for milled OLC (1.4/1.2) after milling. This minor change is indicating a merely light increase in defect density. This supports the results reported by Lee *et al.*[34] and Reinert *et al.*,[35] where different setups were used to disperse OLC. High-resolution transmission electron microscopy measurements (HRTEM) underline these observations as they show that the primary structure of OLC (Figure 2B) is conserved for the milled OLC (Figure 2C) in the ink. The obtained high weight fraction in the colloidal formulation and the structural stability of OLC in the dispersion enables their use as functional carbon additive for inks.

To deposit the OLC-based ink, the small size of the OLC primary particles brings two beneficial features. First, small particles are required for inks to prevent nozzle clogging. Literature provides a rule of thumb limiting the maximal particle size to 1/50 of the nozzle diameter. Here, this can be translated to a maximum size of 3 μm for the inkjet printing and 1 μm for spraying. Second, the small primary particles entail a high surface to weight ratio, which is a key parameter for capacitive energy storage materials. The packing of spherical OLC particles results in a mesoporous electrode offering high accessibility and a big reservoir of electrolyte, which is beneficial for the reactance of the system especially at high scan rates. Despite the presence of SDS in the electrode, the mesoporous structure remains accessible, which can be derived from nitrogen sorption measurements (Figure S5). The ink could be deposited via piezoelectric spraying and with the addition of DSMO also by inkjet technique. Differences in both techniques, which affect the electrode morphology, are revealed by SEM measurements (Figure 3, Figure S8, Figure S9).

The sprayed electrode possesses a rough surface (Figure 3A) with inhomogeneities in the range of a few micrometers. This structure is a result of the fast coating process to a specific mass of around 0.5 mg cm^{-2} within 25 minutes. The substrate was heated to promote fast solvent evaporation enabling the fast rate of deposition. During the final steps of deposition, the solvent evaporation decelerated as a result of the growing

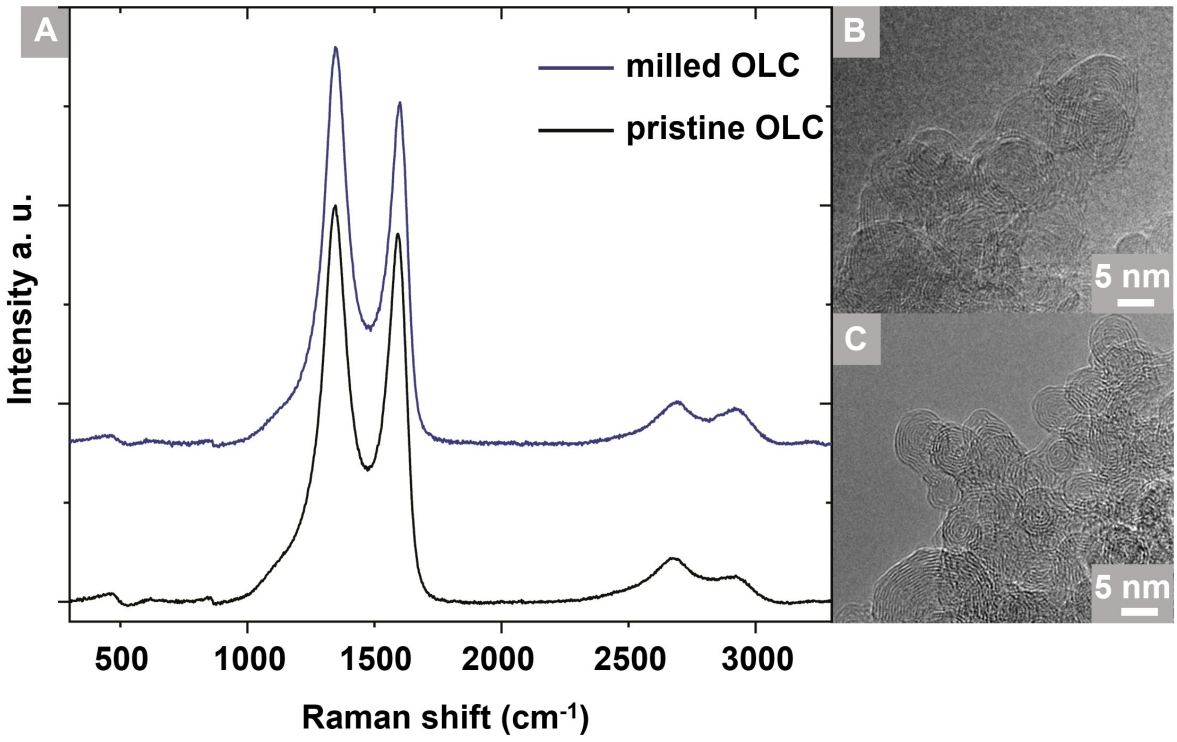

Figure 2. Comparison between milled OLC and pristine OLC in Raman spectroscopy (A) and HRTEM measurements (B: pristine OLC, C: milled OLC).

Research Article
doi.org/10.1002/batt.202400203
Chemistry Europe
European Chemical Societies Publishing

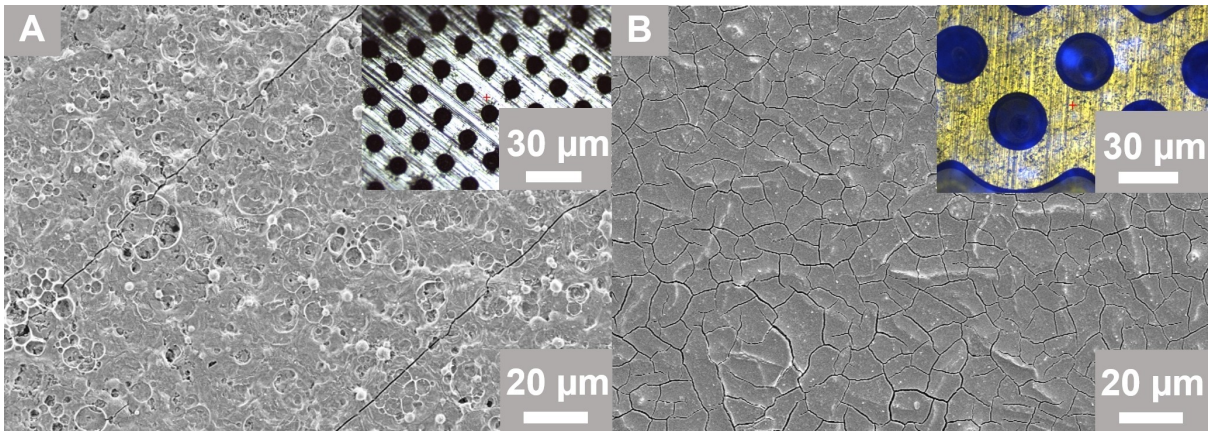

Figure 3. Electrode surface shown by SEM measurement for spray- (A) and inkjet-printed (B) electrodes. The insert shows reflected light microscope images of the respective nozzle used for deposition.

thickness of the coating. This oversaturation with solvent resulted in coffee stain features and inhomogeneities in the form of channels extending deeply into the coating (Figure S6). The inkjet-printed electrode (Figure 3B) did not show this behavior. The homogeneous surface can be explained by the addition of DMSO as an additive in the ink to decrease capillary stress during solvent evaporation.[45] The addition of DMSO required a 10-minute break between every printing cycle, allowing the removal of the majority of the solvent, thus prolonging the process significantly. The cracks in the surface that are visible in the SEM measurement are caused by stress introduced bending of the substrate while it was fed through the printer. This cracking can be prevented in industry-type printer setups. Despite the cracks, no delamination of active material was observed, even after bending the electrode (Figure S4), demonstrating a good flexibility the connection between active material and current collector.

After investigating the morphology of the inkjet-printed and sprayed electrodes, their electrochemical performance was assessed by measurements in a symmetrical two-electrode configuration, in order to ensure comparability with the existing literature.[40,46–47] This setup also allowed the repolarization of the electrode between −2.5 and 2.5 V, featuring a cathodic as well as an anodic charging and discharging process for every cycle. In order to address the different requirements for actual applications of supercapacitors, a wide range of scan rates was investigated by cyclic voltammetry (Figure 4).

Independent from the deposition technique, the electrodes show a quasi-rectangular shape of the voltammograms, which turns into an ellipsoid at high scan rates and increased current densities. The shape of the CV curves demonstrates that the energy is stored in form of an electric double layer capacitance for both deposition techniques. It is observed that the current response at the potential limits is more pronounced for the sprayed electrodes suggesting ongoing charge storage processes that are not directly attributed to the electrical double layer. These processes could be caused by the tortuosity of the active material, with sites only available at elevated potentials or additional electrochemically active sites like functional groups. This could be further explained by a more disordered and less electrically connected structure of the sprayed electrode as observed by SEM measurements (Figure S9).

To evaluate the performance of the differently assembled electrodes, the specific capacitance of the two electrode types was compared (Figure 5A). A mass loading of about 0.5 mg cm^{-2} was deposited in both techniques.

The sprayed and the printed electrodes offer similar specific capacitances of 11 mF cm^{-2} for inkjet-printed coatings and 14 mF cm^{-2} for spray coating at a scan rate of 0.01 V s^{-1}. The specific capacitance decreases with increasing scan rate illustrating kinetic limitations providing values of around 1 mF cm^{-2} at 50 V s^{-1} in both systems. As the rate of polarity change increases alongside the scan rate, the timescale of electrolyte adsorption at the active material's surface is concurrently reduced, leading to a reduction of the specific capacitance (as demonstrated by Figure 5B). An improvement in capacitance could be achieved by increasing the initial surface area of OLC, for example, by introducing micropores through a chemical or thermal activation process.

Slight differences in capacitance between the two electrode types at lower scan rates suggest a higher useable surface for the electrolyte inside the pores of the sprayed electrode compared to the printed electrode. This difference in capacitance originates from a different morphology in both types of electrodes, which is supported by the gravimetric capacitance (24 F g^{-1} for printed and 27 F g^{-1} for sprayed electrodes at 0.01 V s^{-1}, Figure S7). The reduced availability and accessibility of the printed electrode surface could be explained by the closure of cracks after pressing the electrodes (Figure S8). In contrast, the sprayed electrode was affected less by pressing (Figure S9) and could maintain a higher area available for the electrolyte to develop an electric double layer necessary for charge storage. This trend vanishes/inverts at scan rates above 1 V s^{-1}, where the effect of electrical connectivity or a lower ion diffusion resistance could be favorable in a dense structure offered by the inkjet-printed electrodes.

The frequency response behavior of both electrodes was investigated by electrochemical impedance spectroscopy (Fig-

Research Article
doi.org/10.1002/batt.202400203
Chemistry Europe
European Chemical Societies Publishing

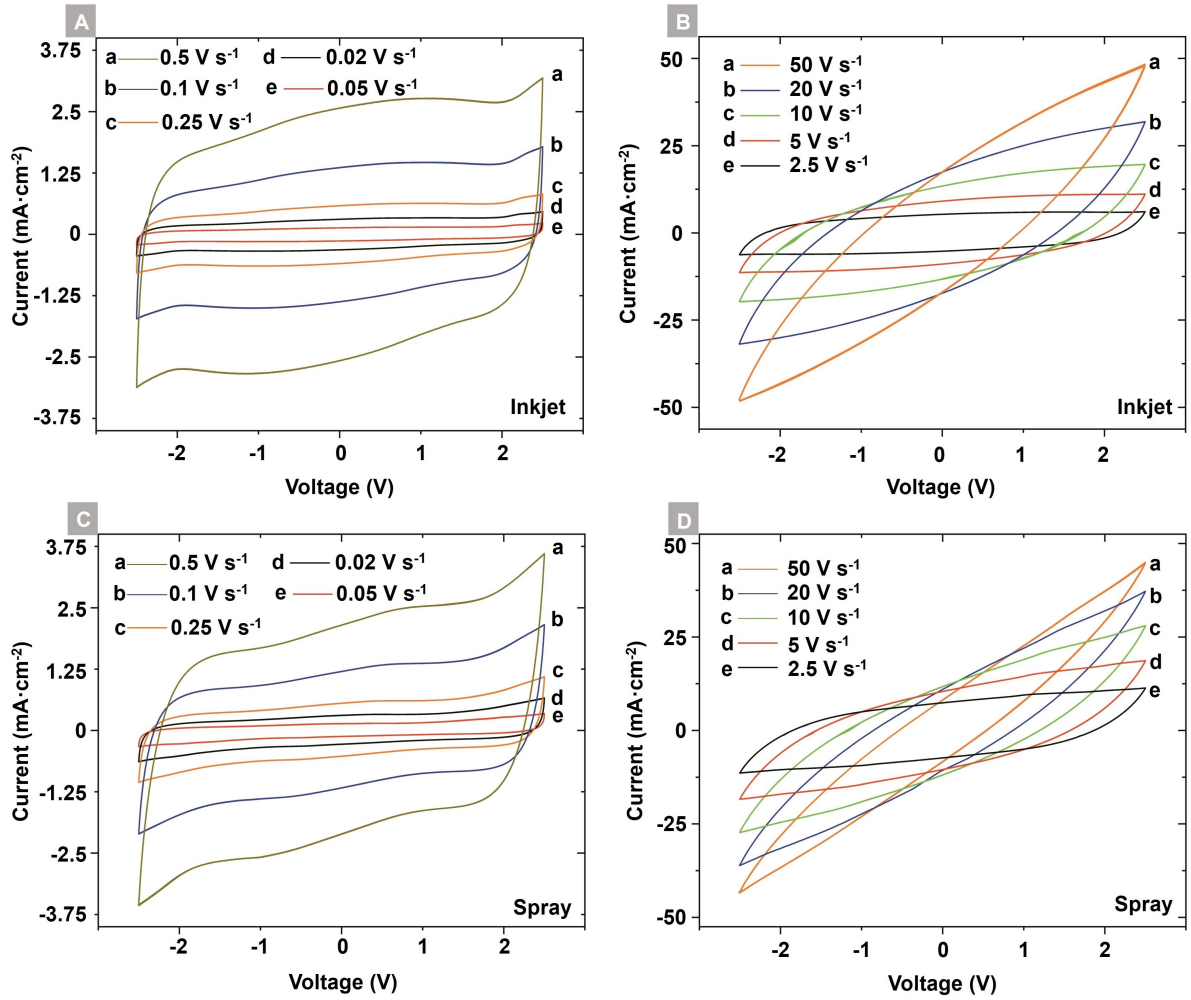

Figure 4. Cyclic voltammetry measurements of the electrodes produces by inkjet printing (A and B) and sprayed electrodes (C and D) at different scan rates from 0.02 $V s^{-1}$ up to 50 $V s^{-1}$.

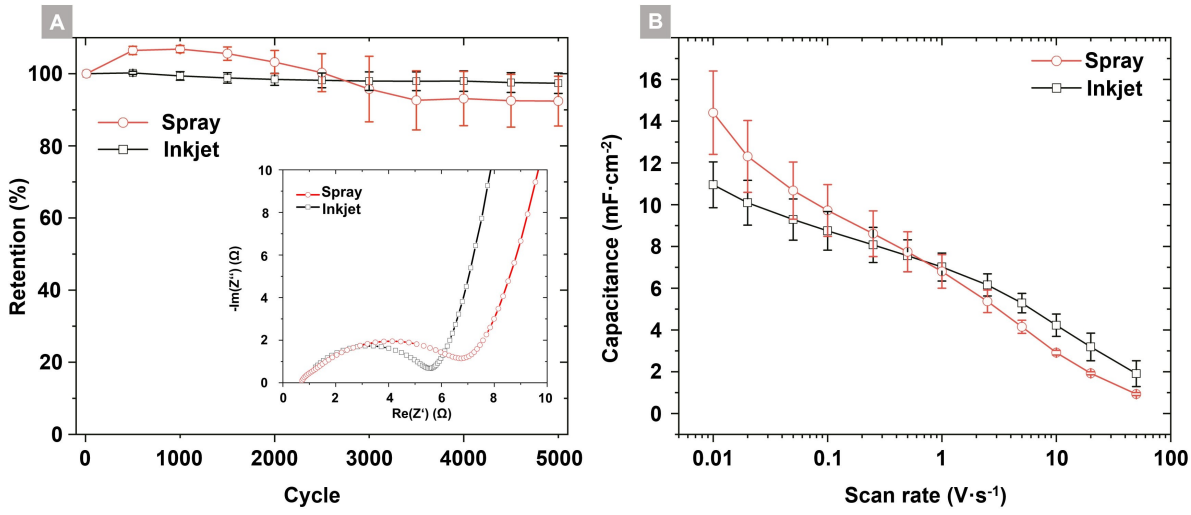

Figure 5. Comparison between the OLC-based electrodes deposited by inkjet printing and spraying technique regarding their long-term stability with an insert showing EIS data (A) and their capacitance at different scan rates (B).

ure 5A). At high frequencies, the Nyquist plot of the printed electrode reveals a higher equivalent series resistance (ESR) of 1.2 Ω compared to 0.7 Ω for the sprayed electrode. This indicates a higher Ohmic resistance of the printed electrode,

caused by the higher number of cracks on the surface (Figure 3B). Conversely, the observed semicircle for the printed electrode in the medium frequency regime has a reduced diameter compared to the plot of the sprayed electrode. The semicircle represents the current passing through the charge transfer resistance (CTR) and the double layer capacitance of the system. Subsequently, the CTR of 4.4 Ω for the printed electrode compared to 6.0 Ω of the sprayed electrode and the shift in the low frequency regime imply lower ion diffusion resistance and a better pore accessibility.[48] This suggests superior behavior at elevated scan rates, which corresponds to the calculated scan rate dependent capacitances (Figure 5B).

To test the long-term stability of the electrodes, the cells were cycled 5000 times with a scan rate of 2.5 $V s^{-1}$ (Figure 5B). The inkjet-printed electrodes reached a retention of 97% of their initial capacitance after the test. For spray coated electrodes, fluctuations between 107% after 1000 cycles and 92% after 5000 cycles were recorded. These fluctuations could originate from rearrangement processes of inhomogeneities in the coating during cycling. For example, some of the channels (Figure S6) could be clogged by surfactant, which is slowly solved in the acetonitrile during cycling. This results in an access to new pores at a higher capacitance. This could change in ion diffusion resistance, confirming the findings from EIS. Even though the capacitance retention of the inkjet-printed electrode was more consistent during the stability test, both systems offered a comparable overall electrochemical performance, as is known for non printed OLC electrodes in the literature.[47,49] This qualifies the OLC-based ink in combination with the spray and inkjet printing techniques for future usage in the field of device fabrication. In addition, the performance of the devices can compete with printed supercapacitors made of other carbon nanomaterials such as multiwall carbon nanotubes or graphene. A detailed comparison of the electrochemical performance with similar systems from literature can be found in the supporting information (Table S1).

Conclusions

In summary, we have developed an easily scalable approach for the production of high performance supercapacitor electrodes using the deposition of functional inks based on OLC. With water as solvent and onion-like carbon as active material, the presented ink is based on sustainable components. An outstanding ink stability and high active material concentration of 1 wt.% was achieved using SDS as surfactant in combination with physical deagglomeration by attrition milling. The ink was deposited via spray and inkjet techniques, demonstrating versatility and compatibility in terms of industrial methodology. The obtained electrodes showed capacitances of 14 $mF cm^{-2}$ for sprayed electrodes and 11 $mF cm^{-2}$ for inkjet-printed electrodes. The performance of the electrodes was demonstrated in a wide voltage window of ±2.5 V and at different scan rates ranging from 0.01 to 50 $V s^{-1}$. The storage capabilities were further supplemented with a high stability of the electrodes retaining 97% (inkjet printing) and 92% (spray coating) of their initial capacitance after 5000 cycles.

The developed ink in combination with the low-cost and scalable deposition techniques of inkjet printing and spraying provides an easy to integrate solution to efficiently produce high-performance electrodes for future energy storage applications.

Acknowledgements

The financial support of this project by the Bavarian State Ministry of the Environment and Consumer Protection is gratefully acknowledged (TNT01NaT-72356 "Umweltverträgliche Anwendungen der Nanotechnologie weiterentwickeln: Na + Nano-Batterie"). We thank the Fraunhofer Institute for Silicate Research for access to the potentio-/galvanostat and Lukas Gold for the introduction to the operation of the setup. We acknowledge Martin Kamp for the measurement of the transmission electron micrographs and Andreas Riedl for the provision of a printer head. Open Access funding enabled and organized by Projekt DEAL.

Conflict of Interests

The authors declare no conflict of interest.

Data Availability Statement

The data that support the findings of this study are available from the corresponding author upon reasonable request.

[1] I. Colak, S. Sagiroglu, G. Fulli, M. Yesilbudak, C.-F. Covrig, *Renewable Sustainable Energy Rev.* **2016**, *54*, 396–405.
[2] X. Fan, B. Liu, J. Ding, Y. Deng, X. Han, W. Hu, C. Zhong, *Batteries & Supercaps* **2020**, *3*, 1262–1274.
[3] G. Hu, J. Kang, L. W. T. Ng, X. Zhu, R. C. T. Howe, C. G. Jones, M. C. Hersam, T. Hasan, *Chem. Soc. Rev.* **2018**, *47*, 3265–3300.
[4] H. W. Choi, D.-W. Shin, J. Yang, S. Lee, C. Figueiredo, S. Sinopoli, K. Ullrich, P. Jovančić, A. Marrani, R. Momentè, J. Gomes, R. Branquinho, U. Emanuele, H. Lee, S. Y. Bang, S.-M. Jung, S. D. Han, S. Zhan, W. Harden-Chaters, Y.-H. Suh, X.-B. Fan, T. H. Lee, M. Chowdhury, Y. Choi, S. Nicotera, A. Torchia, F. Mañosa Moncunill, V. Garcia Candel, N. Durães, K. Chang, S. Cho, C.-H. Kim, M. Lucassen, A. Nejim, D. Jiménez, M. Springer, Y.-W. Lee, S. N. Cha, J. I. Sohn, R. Igreja, K. Song, P. Barquinha, R. Martins, G. A. J. Amaratunga, L. G. Occhipinti, M. Chhowalla, J. M. Kim, *Nat. Commun.* **2022**, *13*, 814.
[5] A. Olabi, C. Onumaegbu, T. Wilberforce, M. Ramadan, M. A. Abdelkareem, A. H. Al-Alami, *Energy (Oxf.)* **2021**, *214*, 118987.
[6] S. K. Garlapati, M. Divya, B. Breitung, R. Kruk, H. Hahn, S. Dasgupta, *Adv. Mater.* **2018**, *30*, 1707600.
[7] M. Cheng, R. Deivanayagam, R. Shahbazian-Yassar, *Batteries & Supercaps* **2020**, *3*, 130–146.
[8] Q. Wang, G. Zhang, H. Zhang, Y. Duan, Z. Yin, Y. Huang, *Adv. Funct. Mater.* **2021**, *31*, 2100857.
[9] R. F. Hossain, M. Min, L.-C. Ma, S. R. Sakri, A. B. Kaul, *NPJ 2D Mater. Appl.* **2021**, *5*, 1–12.
[10] C. Sriprachuabwong, C. Karuwan, A. Wisitsorrat, D. Phokharatkul, T. Lomas, P. Sritongkham, A. Tuantranont, *J. Mater. Chem.* **2012**, *22*, 5478–5485.

[11] P. He, J. Brent, H. Ding, J. Yang, D. Lewis, P. O'Brien, B. Derby, *Nanoscale* **2018**, *10*, 5599–5606.
[12] S. Ali, A. Hassan, G. Hassan, J. Bae, C. H. Lee, *Carbon* **2016**, *105*, 23–32.
[13] F. Schackmar, H. Eggers, M. Frericks, B. S. Richards, U. Lemmer, G. Hernandez-Sosa, U. W. Paetzold, *Adv. Mater. Technol.* **2021**, *6*, 2000271.
[14] D. Dodoo-Arhin, R. C. T. Howe, G. Hu, Y. Zhang, P. Hiralal, A. Bello, G. Amaratunga, T. Hasan, *Carbon* **2016**, *105*, 33–41.
[15] S. K. Mondal, A. Biswas, J. R. Pradhan, S. Dasgupta, *Small Methods* **2021**, *5*, 2100634.
[16] X. Li, X. Wang, J. Deng, M. Li, S. Shao, J. Zhao, *Carbon* **2022**, *191*, 267–276.
[17] C. Gellrich, Y. Bräuniger, R. Schmidt, J. Grothe, S. Kaskel, *Batteries & Supercaps* **2024**, *7*, e202300469.
[18] S. Tagliaferri, G. Nagaraju, A. Panagiotopoulos, M. Och, G. Cheng, F. Iacoviello, C. Mattevi, *ACS Nano* **2021**, *15*, 15342–15353.
[19] B. Yao, H. Peng, H. Zhang, J. Kang, C. Zhu, G. Delgado, D. Byrne, S. Faulkner, M. Freyman, X. Lu, *Nano Lett.* **2021**, *21*, 3731–3737.
[20] D. Pech, M. Brunet, H. Durou, P. Huang, V. Mochalin, Y. Gogotsi, P.-L. Taberna, P. Simon, *Nat. Nanotechnol.* **2010**, *5*, 651–654.
[21] Z.-S. Wu, Z. Liu, K. Parvez, X. Feng, K. Müllen, *Adv. Mater.* **2015**, *27*, 3669–3675.
[22] M. Salanne, B. Rotenberg, K. Naoi, K. Kaneko, P.-L. Taberna, C. P. Grey, B. Dunn, P. Simon, *Nat. Energy* **2016**, *1*, 1–10.
[23] X. Wu, R. Liu, J. Zhao, Z. Fan, *Nano Mater. Sci.* **2021**, *3*, 241–267.
[24] R. Kumar, E. Joanni, S. Sahoo, J.-J. Shim, W. K. Tan, A. Matsuda, R. K. Singh, *Carbon* **2022**, *193*, 298–338.
[25] M. Zeiger, N. Jäckel, M. Aslan, D. Weingarth, V. Presser, *Carbon* **2015**, *84*, 584–598.
[26] M. Zeller, V. Lorrmann, G. Reichenauer, M. Wiener, J. Pflaum, *Adv. Energy Mater.* **2012**, *2*, 598–605.
[27] V. L. Kuznetsov, A. L. Chuvilin, Y. V. Butenko, I. Y. Mal'kov, V. M. Titov, *Chem. Phys. Lett.* **1994**, *222*, 343–348.
[28] M. Zhao, H. Song, X. Chen, W. Lian, *Acta Mater.* **2007**, *55*, 6144–6150.
[29] O. Mykhailiv, H. Zubyk, M. E. Plonska-Brzezinska, *Inorg. Chim. Acta* **2017**, *468*, 49–66.
[30] C. Portet, G. Yushin, Y. Gogotsi, *Carbon* **2007**, *45*, 2511–2518.
[31] M. Zeiger, N. Jäckel, V. N. Mochalin, V. Presser, *J. Mater. Chem. A* **2016**, *4*, 3172–3196.
[32] A. D. C. Permana, A. Omar, I. G. Gonzalez-Martinez, S. Oswald, L. Giebeler, K. Nielsch, D. Mikhailova, *Batteries & Supercaps* **2022**, *5*, e202100353.
[33] K. L. Van Aken, K. Maleski, T. S. Mathis, J. P. Breslin, Y. Gogotsi, *ECS J. Solid State Sci. Technol.* **2017**, *6*, M3103.
[34] J.-Y. Lee, K.-H. Cho, D.-P. Lim, Y.-B. Lee, D.-S. Lim, *Appl. Phys. A* **2007**, *88*, 693–697.
[35] L. Reinert, M. Zeiger, S. Suarez, V. Presser, F. Mücklich, *RSC Adv.* **2015**, *5*, 95149–95159.
[36] A. Krueger, M. Ozawa, G. Jarre, Y. Liang, J. Stegk, L. Lu, *Phys. Status Solidi A* **2007**, *204*, 2881–2887.
[37] M. Ozawa, M. Inaguma, M. Takahashi, F. Kataoka, A. Krüger, E. Ōsawa, *Adv. Mater.* **2007**, *19*, 1201–1206.
[38] Y. Liu, R. L. Vander Wal, V. N. Khabashesku, *Chem. Mater.* **2007**, *19*, 778–786.
[39] A. Childress, K. Ferri, A. M. Rao, *Carbon* **2018**, *140*, 377–384.
[40] D. T. Pham, T. H. Lee, D. H. Luong, F. Yao, A. Ghosh, V. T. Le, T. H. Kim, B. Li, J. Chang, Y. H. Lee, *ACS Nano* **2015**, *9*, 2018–2027.
[41] Y. Liang, M. Ozawa, A. Krueger, *ACS Nano* **2009**, *3*, 2288–2296.
[42] K. L. Van Aken, J. K. McDonough, S. Li, G. Feng, S. M. Chathoth, E. Mamontov, P. F. Fulvio, P. T. Cummings, S. Dai, Y. Gogotsi, *J. Phys. Condens. Matter* **2014**, *26*, 284104.
[43] G.-p. Wang, M. Li, Y. Qian, L.-f. Jia, Y.-q. Tao, J. Qi, X. Lu, *Int. J. Electrochem. Sci.* **2021**, *16*.
[44] C. Knieke, A. Berger, M. Voigt, R. N. K. Taylor, J. Röhrl, W. Peukert, *Carbon* **2010**, *48*, 3196–3204.
[45] M. Schneider, J. Maurath, S. B. Fischer, M. Weiß, N. Willenbacher, E. Koos, *ACS Appl. Mater. Interfaces* **2017**, *9*, 11095–11105.
[46] M. Salihovic, P. Schlee, S. Herou, M.-M. Titirici, N. Hüsing, M. S. Elsaesser, *ACS Appl. Energ. Mater.* **2021**, *4*, 11183–11193.
[47] M. Zeiger, N. Jäckel, D. Weingarth, V. Presser, *Carbon* **2015**, *94*, 507–517.
[48] B.-A. Mei, O. Munteshari, J. Lau, B. Dunn, L. Pilon, *J. Phys. Chem. C* **2018**, *122*, 194–206.
[49] C. Bauer, A. Bilican, S. Braxmeier, G. Reichenauer, A. Krueger, *Carbon* **2022**, *197*, 555–562.

Manuscript received: March 24, 2024
Revised manuscript received: April 23, 2024
Accepted manuscript online: April 27, 2024
Version of record online: June 4, 2024